

Band Expansion-Based Over-Complete Independent Component Analysis for Multispectral Processing of Magnetic Resonance Images

Yen-Chieh Ouyang, *Member, IEEE*, Hsian-Min Chen, Jyh-Wen Chai, Clayton Chi-Chang Chen*, Sek-Kwong Poon, Ching-Wen Yang, San-Kan Lee, and Chein-I Chang, *Senior Member, IEEE*

Abstract—Independent component analysis (ICA) has found great promise in magnetic resonance (MR) image analysis. Unfortunately, two key issues have been overlooked and not investigated. One is the lack of MR images to be used to unmix signal sources of interest. Another is the use of random initial projection vectors by ICA, which causes inconsistent results. In order to address the first issue, this paper introduces a band-expansion process (BEP) to generate an additional new set of images from the original MR images via nonlinear functions. These newly generated images are then combined with the original MR images to provide sufficient MR images for ICA analysis. In order to resolve the second issue, a prioritized ICA (PICA) is designed to rank the ICA-generated independent components (ICs) so that MR brain tissue substances can be unmixed and separated by different ICs in a prioritized order. Finally, BEP and PICA are combined to further develop a new ICA-based approach, referred to as PICA-BEP to perform MR image analysis.

Manuscript received February 25, 2007; revised April 27, 2007 and September 17, 2007. This work was supported in part by the National Science Council, Taiwan, under Grant NSC 96-2221-E-075A-001-MY3 and in part by the Taichung Veterans General Hospital under Grant TCVGH-NCHU 967613. Asterisk indicates corresponding author.

Y.-C. Ouyang is with the Department of Electrical Engineering, National Chung Hsing University, Taichung 402, Taiwan, R.O.C. (e-mail: ycouyang@nchu.edu.tw).

H.-M. Chen is with the Department of Electrical Engineering, National Chung Hsing University, Taichung 402, Taiwan, R.O.C., and also with the Department of Radiology, China Medical University Hospital, Taichung 404, Taiwan, R.O.C. (e-mail: hsianmin@mail.cmuh.org.tw).

J.-W. Chai is with the Department of Radiology, College of Medicine, China Medical University, Taichung 404, Taiwan, R.O.C., and also with the School of Medicine, National Yang-Ming University, Taipei 112, Taiwan, R.O.C., and the Department of Radiology, Taichung Veterans General Hospital, Taichung 407, Taiwan, R.O.C. (e-mail: hubt@vghc.gov.tw).

*C. C.-C. Chen is with the Department of Radiological Technology, Central Taiwan University of Science and Technology, Taichung 406, Taiwan, R.O.C., and also with the Department of Physical Therapy, National Yang-Ming University, Taipei 112, Taiwan, R.O.C., and with the Department of Physical Therapy, Hung Kuang University, Taichung 406, Taiwan R.O.C., and with the Department of Radiology, Taichung Veterans General Hospital, Taichung 407, Taiwan, R.O.C. (e-mail: ccc@vghc.gov.tw).

S.-K. Poon is with the Division of Gastroenterology, Department of Internal Medicine, Center of Clinical Informatics Research Development, Taichung Veterans General Hospital, Taichung 407, Taiwan, R.O.C. (e-mail: fskpoon@gmail.com).

C.-W. Yang is with the Computer and Communications Center, Taichung Veterans General Hospital, Taichung 407, Taiwan, R.O.C. (e-mail: cwyang@vghc.gov.tw).

S.-K. Lee is with Chia Yi Veterans Hospital, Chia Yi 600, Taiwan, R.O.C., and also with the National Defense Medical Center, Taipei 114, Taiwan, R.O.C., and Chung Shan Medical University, Taichung 402, Taiwan, R.O.C. (e-mail: sklee@mail.vhcy.gov.tw).

C.-I. Chang is with the Remote Sensing Signal and Image Processing Laboratory, Department of Computer Science and Electrical Engineering, University of Maryland, Baltimore, MD 21250 USA, and also with the Environmental Restoration and Disaster Reduction Research Center and Department of Electrical Engineering, National Chung Hsing University, Taichung 402, Taiwan, R.O.C. (e-mail: cchang@umbc.edu).

Digital Object Identifier 10.1109/TBME.2008.919107

Index Terms—Band-expansion process (BEP), FastICA, independent component analysis (ICA), magnetic resonance (MR) analysis, over-complete ICA (OC-ICA), prioritized ICA (PICA), prioritized ICA band-expansion process (PICA-BEP).

I. INTRODUCTION

INDEPENDENT component analysis (ICA) has shown great success in functional magnetic resonance imaging (fMRI), which is a method that provides functional information of magnetic resonance (MR) images in time series as a temporal function [1]. Recently, a new application of ICA to MR image (MRI) analysis was investigated by Nakai *et al.* in [2] for contrast enhancement of gray matter (GM) and white matter (WM). A major difference between fMRI and MRI analysis is the mixing matrix to be used by ICA for signal source separation. Since the samples for fMRI are collected along a temporal sequence with the number of samples, denoted by L , generally greater than the number of sources to be separated, denoted by p , the ICA implemented in fMRI is actually under-complete in the sense that ICA deals with under representation of a mixed model, referred to as under-complete ICA (UC-ICA). Under such circumstance, the ICA intends to solve an over-determined system with L equations specified by the number of samples and p unknowns represented by signal sources to be separated, and there will be no solutions for $L > p$ in general, because more than one independent component (IC) must be used to accommodate a single signal source. This may be one reason that UC-ICA generally requires dimensionality reduction (DR). By contrast, the samples used for MRI analysis are a stack of images acquired by different pulse sequences specified by three MR tissue parameters, spin-lattice (T_1), spin-spin (T_2) relaxation times, and proton density (PD). So, generally speaking, these three images, T_1 weighted, T_2 weighted, and PD weighted, can be used for MRI analysis. If the number of signal sources to be separated p is greater than the number of different combinations of pulse sequences, L with $L < p$, then one IC must be used to accommodate more than one signal source. In this case, ICA must deal with an under-determined system using an over-complete representation of a mixed model, referred to as over-complete ICA (OC-ICA). Accordingly, fMRI and MRI analysis are essentially different applications and approaches developed for one application usually cannot be directly applied to another. However, in order to take advantage of ICA implemented as UC-ICA in the same way that it is applied to the fMRI, Nakai *et al.* assumed that the number of sensors L is greater than or equal to the

number of sources p , where the number of sensors corresponds to the combinations of acquisition parameters echo time (TE) and repetition time (TR), and a signal source is represented by a tissue cluster characterized by a unique combination of T1 and T2 relaxation times. Using the changes in signal intensity of each tissue cluster reflected by combinations of TR and TE before and after an ICA transform, the contrast resulting from effects of ICA can be used to perform image evaluation for a particular tissue such as GM and WM. Unfortunately, Nakai *et al.*'s ICA approach overlooked a crucial and important issue. If we interpret the number of pulse sequences used in MR acquisition, denoted by L , and brain tissue substances such as GM and WM, cerebral spinal fluid (CSF), muscle, skin, fat, etc., as signal sources to be separated, denoted by p , the L is actually less than p , not great than p . Consequently, the problem to be solved for MRI analysis is indeed an under-determined system with $L < p$, which violates the key assumption made in Nakai *et al.*'s ICA approach as well as in most ICA-based approaches used for fMRI. Interestingly, little work has been done regarding using OC-ICA to perform MRI analysis. Another issue that was not addressed by Nakai *et al.* is the use of random initial projection vectors by ICA to produce ICs. The problem with this random approach results from the fact that the final sets of projection vectors produced by two distinct random initial projection vectors are generally different. As a consequence, an ICA transform implemented by the same user in different runs or different users at the same time will produce different sets of ICs. This serious inconsistency undermines repeatability of ICA and makes ICA unstable. Additionally, due to the use of random initial projection vectors, the order of ICA-generated ICs is completely random and does not necessarily indicate the significance or importance of an IC. In other words, an IC generated earlier need not be more important than the ones generated later. Consequently, image evaluation must wait until all ICs are generated. This paper is aimed to addressing these two issues and further develops a rather different approach to implementing ICA, OC-ICA to improve Nakai *et al.*'s ICA approach, which is UC-ICA.

First of all, we need to resolve the issue of lacking band images in MRI analysis. Interestingly, an idea called band-expansion process (BEP) proposed by Ren and Chang [3] can be used for this purpose. The BEP makes use of nonlinear functions to create additional band images that capture nonlinear correlations among the original MR images. These newly BEP-generated images are then combined with the original set of MR images to provide sufficient number of band images to convert OC-ICA to UC-ICA so as to satisfy the assumption made by Nakai *et al.*'s ICA approach. The second issue can be addressed by a new concept, called prioritized ICA (PICA), which is originated from a recent work of using ICA to perform DR for hyperspectral imagery [4]. As a result of PICA, ICs can be appropriately prioritized according to different applications. Finally, implementing PICA in conjunction with BEP gives rise to a new approach to be called PICA-BEP, which can implement OC-ICA to perform the same contrast enhancement of GM and WM that was carried out by Nakai *et al.*'s approach using UC-ICA [2].

II. ISSUES OF OVER-COMPLETE ICA

The main key idea behind ICA assumes that data are linearly mixed by a set of separate independent unknown signal sources by which these signal sources can be unmixed according to their statistical independency measured by mutual information. In order to validate its approach, an underlying assumption is that at most one source in the mixture model can be allowed to be a Gaussian source. This is due to the fact that a linear mixture of Gaussian sources is still a Gaussian source. More specifically, let \mathbf{x} be a linearly mixed signal source vector expressed by

$$\mathbf{x} = \mathbf{A}\mathbf{s} \quad (1)$$

where \mathbf{A} is an unknown $L \times p$ mixing matrix and $\mathbf{s} = (s_1, s_2, \dots, s_p)^T$ is also an unknown p -dimensional signal source vector needed to be separated. The goal of ICA is to process the observed mixed signal source \mathbf{x} in (1) and further find an unmixing matrix \mathbf{W} in such a manner that the p unknown signal sources in the signal source vector \mathbf{s} can be separated via a demixing equation [1], [5], [6] given by

$$\mathbf{s} = \mathbf{W}\mathbf{x}. \quad (2)$$

Despite the fact that ICA has found its potential in many applications, it cannot be blindly applied without extra care. In particular, several crucial issues have been overlooked and ignored in fMRI and MRI analysis. One key issue is the mixing matrix \mathbf{A} to be used in the fMRI and MRI analysis. When ICA is applied to fMRI, the signal source is 1-D signal and the used ICA is generally under-complete in which the number of observations L of the mixing matrix \mathbf{A} in (1) is always greater than the number of signal sources p to be unmixed, i.e., $L > p$. In this case, there are no solutions to (1). In order to mitigate this dilemma, a general approach is to use DR such as principal components analysis (PCA) as a preprocessing step to reduce L to p to make the mixing matrix \mathbf{A} a square matrix. By contrast, as ICA is applied to MR images as multispectral images, the signal sources to be unmixed are actually 2-D images rather than 1-D signals considered in fMRI. Therefore, the resulting ICA is indeed over-complete in the sense that the number of MR images, L , used in the mixing matrix \mathbf{A} is smaller than the number of signal signals, p with $L < p$, in which case, one single IC must be used to accommodate multiple signal sources due to the lack of data dimensionality. Because of that, several problems that are never encountered in UC-ICA become major issues in OC-ICA. For example, in MRI analysis, the data dimensionality of L used in the mixing matrix \mathbf{A} represents the number of MR images, which are acquired by pulse sequences such as T1, PD, T2, and the number of signal sources, p used in the \mathbf{A} indicates the number of brain tissue substances of interest such as GM, WM, and CSF, etc. Additionally, there is also noise present in MR images, which requires an additional IC for its accommodation. In this case, the ICA needs at least four ICs to separate the three signal sources, GM, WM, CSF plus noise source. Unfortunately, with only three available MR images, the ICA can only produce three ICs to accommodate four signal sources, GM, WM, CSF, and noise. As expected,

at least two sources must be unmixed into one single IC and cannot be discriminated in this particular IC. Most importantly, the noise can be spread into all three ICs to obscure analysis. Such a phenomenon will not occur in fMRI, but becomes an inevitable issue in MRI analysis, which was not addressed in the past.

Another major problem is caused by the implementation of ICA. In order to initialize an ICA algorithm such as the FastICA developed by Hyvarinen and Oja [6] along with its web site [7], a general approach is to randomly generate a set of projection vectors to converge to a set of final projection vectors that produce desired ICs. However, this results in two major issues. One is the use of random initial projection vectors. The final ICs produced by the ICA are generally different if two different sets of random initial projection vectors are used. This is because noise is completely random and various levels of noise effects can be introduced into different ICs. Furthermore, the orders of ICs produced by ICA are also different if two different sets of random initial projection vector are used. In other words, unlike the PCA that produced the principal components (PCs) in accordance with data variance, the order that ICs appear is completely random and does not provide any indication of the significance of ICs. As a consequence, different users may produce different sets of final ICs or the same user who runs the ICA more than once may have different sets of final ICs. This drawback is particularly severe when there are no sufficient ICs to be used for signal source accommodation or when the data space has been suppressed by data DR. Unfortunately, this issue has never been investigated and explored in MRI analysis.

III. BAND-EXPANSION PROCESS

The BEP presented in this section is developed to resolve the issue of insufficient MR images to be used for MRI analysis. When MR images are considered as multispectral band images, each of these MR band images represents information provided by a different pulse sequence. If we use one MR band image to accommodate one brain tissue substance, the number of substances to be accommodated should not exceed the number of MR band images, which is generally 3. As a matter of fact, in MRI analysis, there are always more than 3 brain tissue substances such as GM, WM, CSF, fat, blood, water, etc., plus noise. The idea of BEP arises from the fact that a second-order random process is generally specified by its first-order and second-order statistics. If we view the original MR bands as random variables, we can generate a set of second-order statistical band images by capturing correlation among different random variables, which are the original MR band images. These correlated band images provide missing but useful second-order statistical information about the original band images. The second-order statistics to be used for BEP include autocorrelation, crosscorrelation, and nonlinear correlation to create nonlinearly correlated images. The concept of producing second-order correlated band images coincides with that used in signal processing to generate covariance functions for a random process. Despite that such band expansion may not have real physical reasoning, it does provide a significant advantage to cope with the issue of insufficient

band images. The idea of implementing BEP can be described as follows.

Band expansion process (BEP)

Step 1) Let $\{B_l\}_{l=1}^L$ be set of original band images

Step 2) Second-order correlated band images:

- i) $\{B_l^2\}_{l=1}^L$ = set of autocorrelated band images
- ii) $\{B_k B_l\}_{k=1, l=1, k \neq l}^{L, L}$ = set of crosscorrelated band images.

In case, a rescaling is needed, auto- or crosscorrelated band images can be normalized by the variances of band images such as $(\sigma_{B_l}^2)^{-1} \{B_l^2\}$ and $(\sigma_{B_k} \sigma_{B_l})^{-1} \{B_k B_l\}$.

Step 3) Nonlinear correlated band images:

- i) $\{\sqrt{B_l}\}_{l=1}^L$ = set of band images stretched out by the square root
- ii) $\{\log(B_l)\}_{l=1}^L$ = set of band images stretched out by the logarithmic function.

It is worth noting that all the band images generated by BEP are produced nonlinearly and provide useful nonlinear spectral information to help to improve performance. However, we should point out that according to our extensive experience, using the crosscorrelated band images generated by step 2(ii) is generally sufficient to implement BEP. Additionally, using autocorrelated band images produced by step 2(i) may sometimes cause nonsingularity problems in matrix computation because they are self-correlated and usually very close to the original images. It is suggested that they should not be used alone and can be only used in conjunction with crosscorrelated band images. This practice is very similar to the fact that a covariance matrix including variances and covariances provides more information than a diagonal matrix, which only includes variances. Besides, high-order statistics can be also used in BEP. But, according to our experiments, second order of statistics is generally sufficient as demonstrated in [3].

IV. PRIORITIZED INDEPENDENT COMPONENT ANALYSIS

In order to address the second issue resulting from the use of random initial projection vectors, a new concept, called PICA to prioritize ICA-generated ICs, is introduced in this section. Three PICA-based algorithms developed in [4], eigenvector-prioritized PICA (Eigen-PICA), high-order statistics-prioritized PICA (HOS-PICA), and automatic target-generation process (ATGP)-prioritized PICA (ATGP-PICA) are developed to implement PICA. Assume that the data dimensionality is L , and there are L ICs generated by the ICA, denoted by $\{IC_i\}_{i=1}^L$.

A. Eigenvector-Prioritized ICA

A simplest way to prioritize ICs is to use eigenvalues as a priority measure. The idea of the Eigen-PICA comes from PCA where its PCs are ordered by data variance. So, the Eigen-PICA takes advantage of eigenvectors of the data matrix, and use these vectors as an initial set of projection vectors for ICA.

1) *Eigen-PICA algorithm:*

1. Find a set of eigenvectors of the data matrix, $\{\mathbf{v}_j\}_{j=1}^L$, arranged in order of magnitude of their corresponding eigenvalues.

2. Use each of $\{\mathbf{v}_j\}_{j=1}^L$ generated in step 1 as an initial projection vector, the FastICA produce $\{\text{IC}_i\}_{i=1}^L$ in accordance with priorities determined by the magnitude of eigenvalues.

It should be noted that eigenvalues are derived from the sample data covariance matrix and represents second-order statistics. As a result, on some occasions the Eigen-PICA may not be as effective as other criteria described in the following.

B. High-Order Statistics-Based PICA

The HOS-PICA is to prioritize ICA-generated ICs whose significance is measured by high-order statistics. Two types of high-order statistics are of major interest, the third-order statistics, referred to as skewness, and the fourth-order statistics, referred to as kurtosis. The algorithm to implement the HOS-PICA is summarized as follows.

1) HOS-PICA algorithm:

1. The FastICA is used to randomly generate a unit vector as an initial projection vector to produce each of ICs.
2. Calculate the third and fourth orders of statistics for ζ_i

$$J(\text{IC}_i) = \kappa_i^3 \text{ or } J(\text{IC}_i) = \kappa_i^4 \quad (3)$$

where $\kappa_i^3 = E[\zeta_i^3] = (1/\text{MN}) \sum_{n=1}^{\text{MN}} (z_n^i)^3$ and $\kappa_i^4 = E[\zeta_i^4] = (1/\text{MN}) \sum_{n=1}^{\text{MN}} (z_n^i)^4$ are sample means of third and fourth orders of statistics in the IC_i .

3. Prioritize the $\{\text{IC}_i\}_{i=1}^L$ in accordance with the magnitude of $J(\text{IC}_i)$.

C. ATGP-Prioritized PCA

The ATGP developed in [3] was developed to find potential target pixels in a hyperspectral imagery. It repeatedly makes use of an orthogonal subspace projector defined in [8] and [9] by

$$P_H^\perp = \mathbf{I} - \mathbf{H}(\mathbf{H}^T \mathbf{H})^{-1} \mathbf{H}^T, \quad \text{for any matrix } \mathbf{H} \quad (4)$$

to find target pixels of interest from the data.

1) Automatic target generation process:

- 1) *Initial condition:* Select an initial target pixel vector of interest denoted by \mathbf{t}_0 , which is a target pixel vector with the maximum length as the initial target \mathbf{t}_0 , namely, $\mathbf{t}_0 = \arg\{\max_r \mathbf{r}^T \mathbf{r}\}$, i.e., the brightest pixel vector in the image scene. Set $k = 1$ and $U_0 = [\mathbf{t}_0]$.
- 2) At n th iteration, apply $P_{\mathbf{t}_0}^\perp$ via (4) with $U = [\mathbf{t}_0]$ to all image pixels \mathbf{r} in the image and find the n th target \mathbf{t}_n generated at the n th stage that has the maximum orthogonal projection as follows.

$$\mathbf{t}_n = \arg \left\{ \max_r \left[\left(P_{[\mathbf{t}_0 \ U_{n-1}]}^\perp \mathbf{r} \right)^T \left(P_{[\mathbf{t}_0 \ U_{n-1}]}^\perp \mathbf{r} \right) \right] \right\} \quad (5)$$

where $U_{n-1} = [\mathbf{t}_1 \ \mathbf{t}_2 \ \dots \ \mathbf{t}_{n-1}]$ is the target matrix generated at the $(n-1)$ st stage.

- 3) *Stopping rule:* If $n < L - 1$, let $U_n = [U_{n-1} \ \mathbf{t}_n] = [\mathbf{t}_1 \ \mathbf{t}_2 \ \dots \ \mathbf{t}_n]$ be the n th target matrix, go to step 2. Otherwise, continue.
- 4) At this stage, the ATGP is terminated and the target matrix is U_{p-1} , which contains $L-1$ target pixel vectors,

$\mathbf{t}_1, \mathbf{t}_2, \dots, \mathbf{t}_{L-1}$, as its column vectors and the initial target pixel vector \mathbf{t}_0 provide an initial set of projection vectors for ICA.

Using the ATGP as an initialization algorithm, the ATGP-PICA can be described as follows.

2) ATGP-PICA algorithm:

1. Use the ATGP to produce set of projection vectors $\{\mathbf{t}_j\}_{j=0}^{L-1}$ arranged in their appearing orders.
2. Use the set of $\{\mathbf{t}_j\}_{j=0}^{L-1}$ generated in step 1 as an initial set of projection vectors for ICA to produce $\{\text{IC}_i\}_{i=1}^L$.

It is worth noting that the previous three PICA-based algorithms are derived from different perspectives and have their own merits. In HOS-PICA, the process of IC prioritization is performed after all the ICs are generated. Unlike HOS-PICA, Eigen-PICA and ATGP-PICA do not need to generate all ICs prior to IC prioritization. In other words, both Eigen-PICA and ATGP-PICA do not wait for all ICs to be generated. Instead, they prioritize ICs while generating the ICs. The priorities of ICs are determined by the order of their used initial projection vectors. As a result, once the set of initial projection vectors is determined, the IC priority is also determined accordingly.

V. EXPERIMENTS

The experiments conducted in this section followed the same manner performed in [2] to demonstrate contrast enhancement of the GM and WM in MRI analysis. Two sets of MR images were used to substantiate the utility of our proposed PICA-BEP in multispectral processing of MR images as well as to demonstrate advantages of PICA-BEP over the traditional ICA used in [2]. One set of images is the data base of MR brain synthetic images available on web site [10] and the other is real MR brain images acquired by using a whole body 1.5 T MR system in the Taichung Veterans General Hospital.

A. Synthetic Brian Image Experiments

The synthetic images to be used for experiments in this section were the axial T1, T2, and proton density MR brain images [with 5-mm section thickness, 0% noise, and 0% intensity nonuniformity (INU)] resulting from the MR imaging simulator of McGill University, Montreal, PQ, Canada (available at www.bic.mni.mcgill.ca/brainweb/). The image volume provided separate volumes of tissue classes such as CSF, GM, WM, bone, fat, and background. The use of these web MR brain images is to allow researchers to reproduce our experiments for verification.

Fig. 1(a) shows three MR brain images with specifications provided in [10] where the first image is acquired by modality = PD, protocol = International Consortium of Brain Mapping (ICBM), phantom name = normal, slice thickness = 5 mm, noise = 0%, INU = 0%, the second image by modality = T1, protocol = ICBM, phantom name = normal, slice thickness = 5 mm, noise = 0%, INU = 0%, and the third image by modality = T2, protocol = ICBM, phantom name = normal, slice thickness = 5 mm, noise = 0%, INU = 0%. Fig. 1(b) provides the ground truth also available on web site [10] for brain

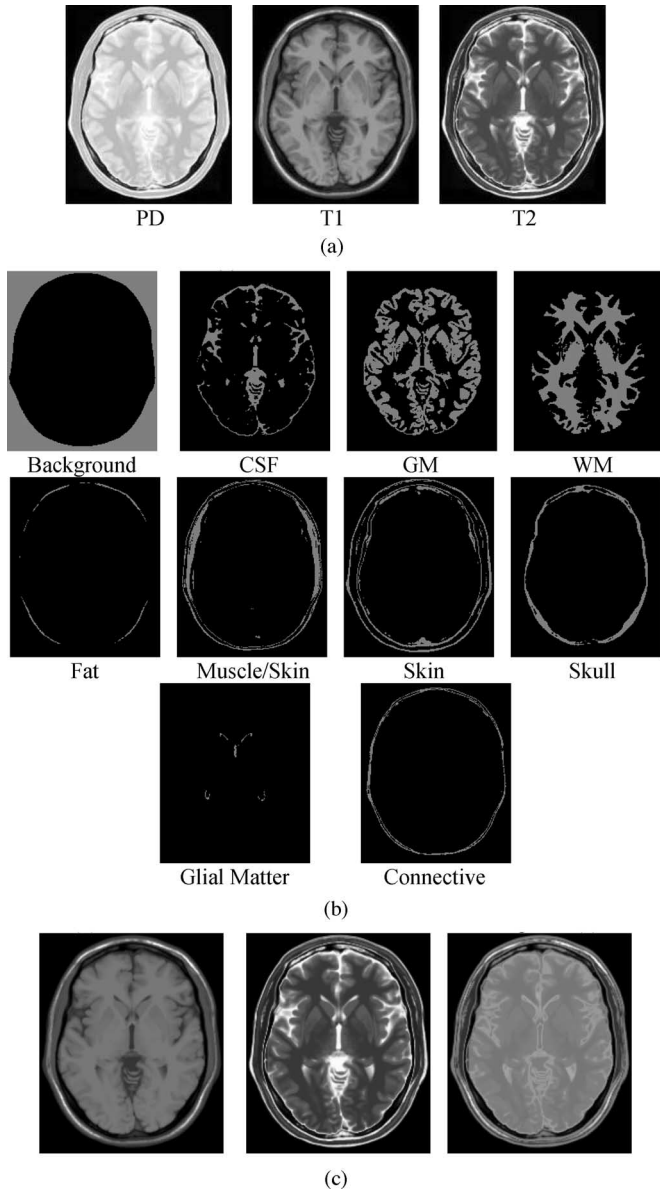


Fig. 1. (a) Three MR synthetic images. (b) Ground truth. (c) Crosscorrelation BEP generated images.

tissue substances in the images in Fig. 1(a), which will be used to verify the results obtained for our experiments.

Fig. 2 shows inability of ICA in separation of the GM, WM, CSF due to insufficient number of MR images where the three ICs could not effectively separate the WM, GM, and CSF. This is because other brain substances had nowhere to go, and were forced to be mixed with the WM, GM, and CSF in only the three ICs. Fig. 2(a)–(c) further demonstrates inconsistent results of ICs resulting from three different sets of random initial projection vectors. In order to address the issue of insufficient MR images, three crosscorrelated images shown in Fig. 1(c) were generated by BEP, and were combined with the original three MR brain images in Fig. 1 to produce six MR images.

Fig. 3 shows the results of six FastICA-generated ICs where the WM, GM, and CSF were successfully separated in individual and separate ICs.

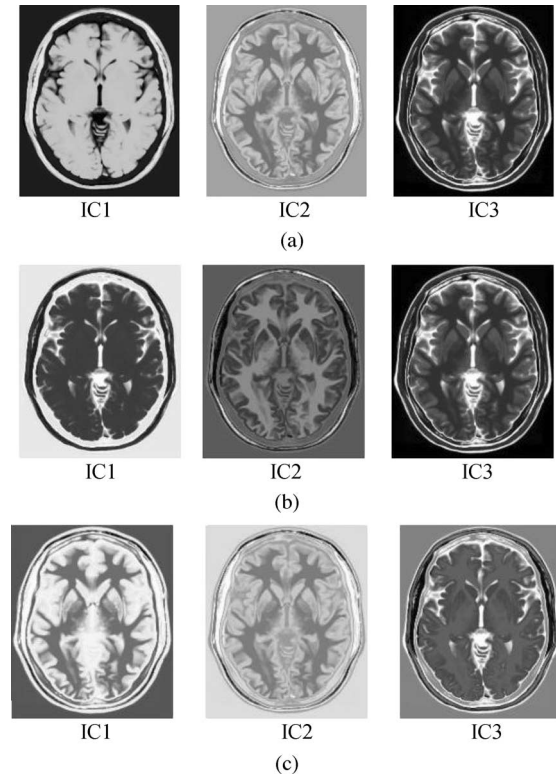


Fig. 2. Three ICs produced by the FastICA using three different sets of random initial projection vectors.

Unfortunately, like Fig. 2, Fig. 3(a)–(c) also shows inconsistent results produced by three different sets of random initial conditions where other brain tissue substances were also separated and identified underneath each of ICs according to the ground truth provided by Fig. 1(b). To resolve this issue, the three PICA-BEP algorithms proposed in Section IV were implemented to prioritize ICs where Fig. 4(a)–(c) shows six FastICA-generated ICs produced by Eigen-PICA-BEP, HOS-PICS-BEP, and ATGP-PICA-BEP, respectively where all the algorithms but the HOS-PICA-BEP using the fourth order successfully separated WM, GM, and CSF in different priorities.

An interesting and rather important observation from Figs. 3 and 4 is noteworthy. The two major brain tissue substances, WM and GM, were separated in the last two ICs in more than half of cases regardless of what initial projection vectors were used. Additionally, among these three substances, the CSF was always separated first. These experiments provided strong evidence that three ICs in Fig. 2 were not sufficient to effectively separate the WM, GM, and CSF. Similar conclusions can be also drawn from experiments for web images with various levels of noise in [10]. Therefore, no results are included here to avoid redundant descriptions.

The experiments conducted earlier demonstrated that the PICA-BEP could significantly improve ability of ICA in MRI analysis. Two comments are worth being mentioned as follows.

- 1) While performing blind source separation by ICA, it should be noted that it can be only effective when the number of ICs is greater than the number of sources to

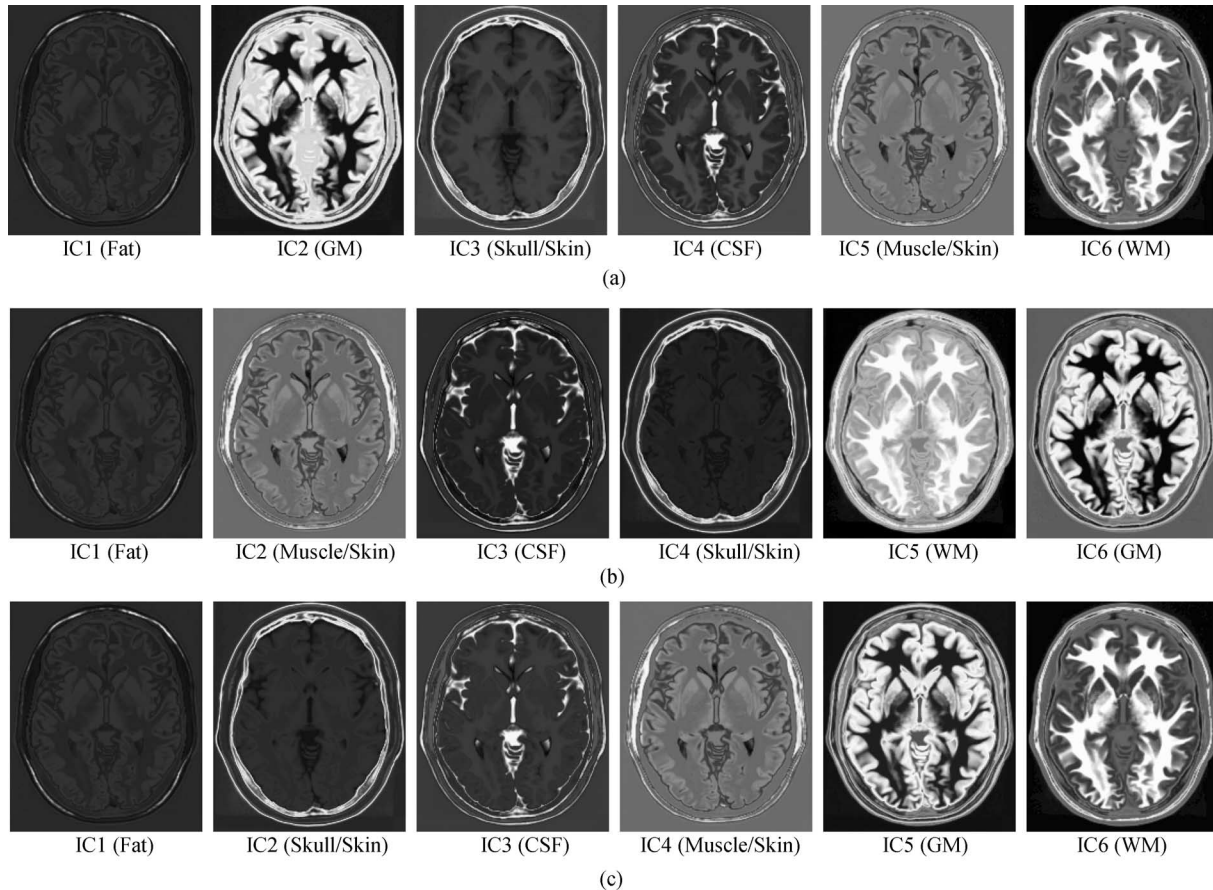


Fig. 3. Six FastICA generated ICs with BEP expanded images using three different sets of random initial projection vectors.

be separated. This was demonstrated in Figs. 2 and 3, where the three major brain tissues, WM, GM, and CSF were mixed in all the three ICs. The introduction of the BEP is developed to mitigate this problem.

- 2) Due to the use of random initial projection vectors, the ICs are generally generated in random orders. As a result, a user who runs ICA in different times or different users who run the IC at the same time produce different results. Such inconsistency makes the ICA unstable and unrepeatable. The PICA-BEP remedies this dilemma by prioritizing all ICs consistently, as demonstrated in Fig. 4.

B. Quantitative Analysis

One great advantage of using the web images in [10] is to allow us to conduct quantitative analysis. According to Fig. 1(b), there are also other brain tissue substances such as skin, fat, glial matter, and background that also constitute different classes. However, from a clinical point of view, only the GM, WM, and CSF are of major interest. Therefore, the MRI quantitative analysis performed in this section was conducted based on contrast enhancement of these three brain tissues in the same way as was done in [2]. In this case, all tissues other than the GM, WM, and CSF were considered as a single class labeled by the background (BKG). However, it should be noted that only the GM and WM were considered, and the CSF was not included for analysis

in [2]. The difficulty of analyzing the CSF in [2] may have resulted from the inability of UC-ICA in dealing with insufficient MR band images. Since ICA is unsupervised, two commonly used unsupervised methods, C-means [11] and fuzzy C-means (FCM) [12], were also used for comparative analysis where the number of classes was set to 4 representing four classes of GM, WM, CSF, and BKG. Finally, because the FastICA-generated ICs are real values, it requires a hard decision maker to threshold each ICs for quantification. In this case, the support vector machine (SVM) [13], [14] was used for this purpose, where nine training samples were selected for each of the four classes, WM, GM, CSF, and BKG. The selection of SVM over other thresholding techniques was because SVM has been shown to be very effective in multiple class classification. It should also be noted that the SVM is a class-labeling process, which converts real values produced by the ICA to hard decisions that assign each data sample to its specific class. As a result, there is no need of thresholding ICs for quantification.

In order to perform quantitative analysis, a quantification measure, called Tanimoto index (TI) defined for multispectral MR images in [11] and [15] as

$$TI = \frac{|A \cap B|}{|A \cup B|} \quad (6)$$

can be used for this purpose where A and B are two data sets and $|X|$ is the size of a set X . According to (6), $TI = 0$ implies

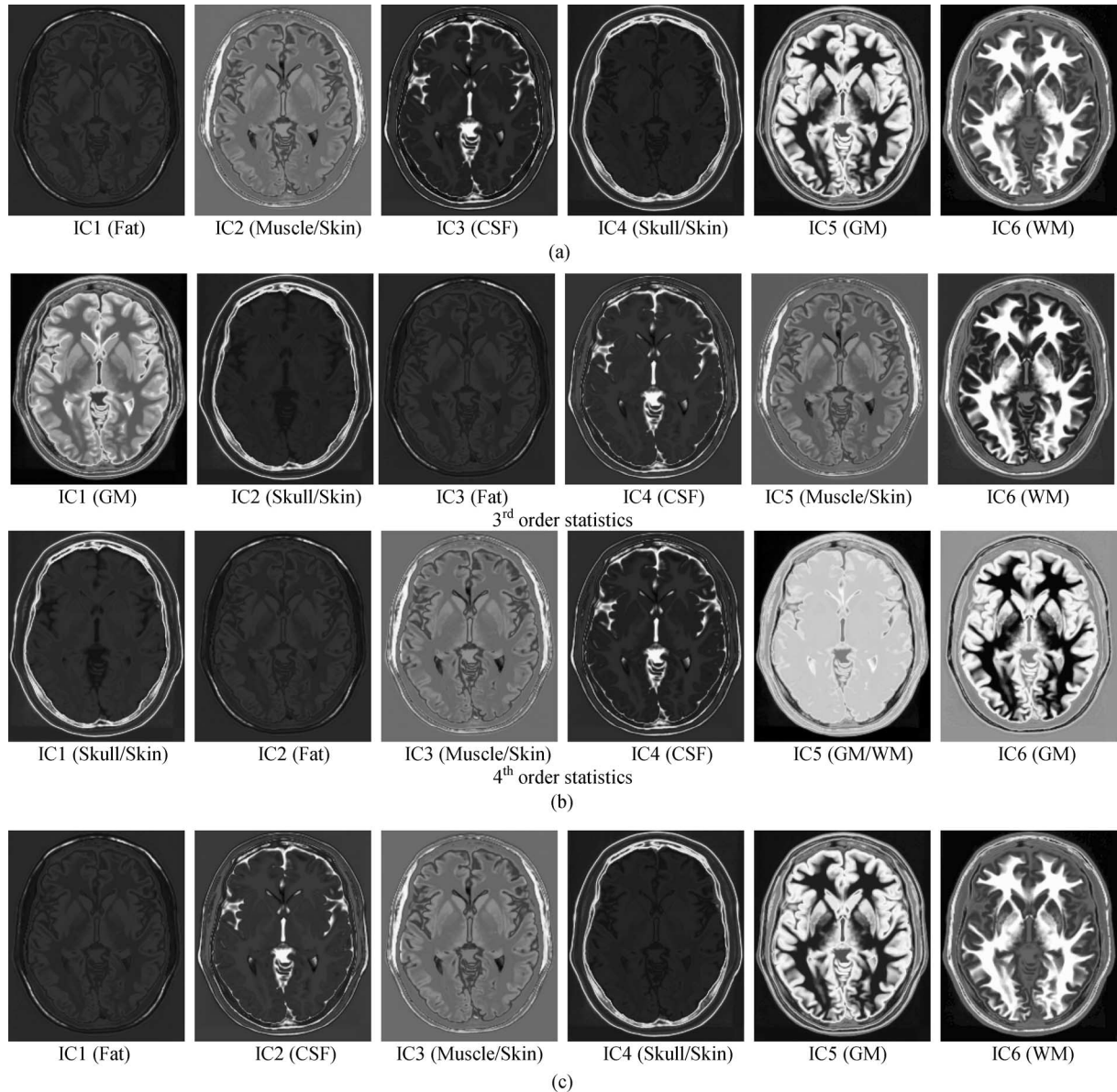


Fig. 4. Results from three PICA-BEP approaches, Eigen-PICA-BEP, HOS-PICA-BEP, ATGP-PICA-BEP.

that both the data sets A and B are completely different, and $TI = 1$ indicates that both the data sets A and B are the same set. Table I(a) and (b) tabulates quantification results of GM, WM, and CSF using MR images with/out BEP, respectively, where TI was the criterion specified by (6) and three methods, PICA with kurtosis, C-means, and FCM were implemented in conjunction with SVM. The “rf” in Table I(a) and (b) indicates the INU defined in [10]. It should be noted that the C-means used random initial conditions. Therefore, its final results were inconsistent due to the same drawback suffered from ICA. In this case, the results of the C-means were obtained by averaging the results of running the C-means ten separate times. Also, since the results obtained by the three PICA algorithms, Eigen-PICA, HOS-PICA, and ATGP-PICA, were similar, only the results using PICA with kurtosis were included in Table I(a) and (b) to avoid redundant tables.

From Table I(a) and (b), several interesting observations can be made.

1. Generally speaking, the FCM method always performed better than the C-means method.
2. Interestingly, the results obtained by both the C-means and FCM methods fusing MR images with/out BEP were close. It implied that BEP did not have much impact on these two methods. In other words, we cannot conclude that one with BEP performed better than another without BEP. This makes sense since both methods are spatial correlation-based methods and have very little to do with linear transformation.
3. Also shown in the table, it seemed that the C-means was the worst and the FCM method was between PICA + SVM with and without BEP. More specifically, the FCM method performed better in separation of CSF and GM, but worse

TABLE I
(a) QUANTIFICATION RESULTS OF GM, WM, AND CSF WITHOUT BEP. (b) QUANTIFICATION RESULTS OF GM, WM, AND CSF WITH BEP

TI	PICA+SVM			C-means			Fuzzy C-means		
	CSF	GM	WM	CSF	GM	WM	CSF	GM	WM
Noise0_rf0	0.4501	0.6435	0.7711	0.4506	0.3063	0.4045	0.4379	0.6320	0.6117
Noise1_rf0	0.4211	0.6243	0.7670	0.4347	0.3215	0.4173	0.4357	0.6300	0.6138
Noise3_rf0	0.4092	0.5960	0.7224	0.4367	0.3226	0.4143	0.4327	0.6142	0.6008
Noise5_rf0	0.4226	0.5763	0.6570	0.4279	0.2885	0.3456	0.4328	0.5942	0.5804
Noise1_rf20	0.4335	0.5981	0.7401	0.4412	0.4007	0.3253	0.4322	0.6282	0.6105
Noise3_rf20	0.3997	0.5259	0.6522	0.4275	0.3488	0.3128	0.4359	0.6157	0.6016
Noise5_rf20	0.4012	0.5862	0.6777	0.4240	0.3374	0.3058	0.4278	0.5969	0.5794

(a)

TI	PICA+SVM			C-means			Fuzzy C-means		
	CSF	GM	WM	CSF	GM	WM	CSF	GM	WM
Noise0_rf0	0.2482	0.6254	0.8053	0.4552	0.3343	0.4656	0.4383	0.6482	0.6074
Noise1_rf0	0.3467	0.7074	0.7780	0.4494	0.4505	0.3997	0.4364	0.6388	0.6086
Noise3_rf0	0.2546	0.6652	0.7340	0.4315	0.4013	0.4326	0.4343	0.6236	0.5925
Noise5_rf0	0.3545	0.5815	0.6187	0.4227	0.2610	0.3830	0.4335	0.5956	0.5691
Noise1_rf20	0.3104	0.6985	0.7409	0.4942	0.3586	0.3181	0.4329	0.6405	0.6028
Noise3_rf20	0.3573	0.6418	0.6738	0.4655	0.2823	0.2986	0.4370	0.6277	0.5895
Noise5_rf20	0.2860	0.6280	0.6399	0.4211	0.1721	0.3066	0.4281	0.5981	0.5655

(b)

in separation of WM than PICA + SVM without BEP. On the other hand, PICA + SVM with BEP performed better the FCM method in separation of GM and WM, but worse in separation of CSF than the FCM method.

- According to [10], the Noise_rf0 simulated in web MR images does not imply that the images are “noise-free.” It simply means that two types of noise are simulated, one with rf20 indicates INU labeled by 20 compared to one with intensity uniformity denoted by rf0. So, the performance for the case of Noise_rf0 was not necessarily the best among all noise cases.
- The performance of all the three methods, PICA + SVM, C-means, and FCM with/without BEP was always degraded by noise level except the case of Noise5_rf0 for separation of CSF. Also, in most of cases, these three methods with/without BEP generally performed worse for MR images with Noise_rf20 than MR images with Noise_rf0.
- PICA-BEP + SVM was more sensitive to Noise_rf20 (i.e., INU) than PICA + SVM without BEP and the other two methods with/without BEP.
- It should be noted that Table I(a) and (b) provides quantification results for the classifiers SVM, C-means, and FCM. The effectiveness of a classifier is determined by a threshold value t , which can be selected according to different applications. For example, if the t is set to 0.5, according to Table I(b), both the GM and WM were successfully detected by PICA + SVM and FCM. However, if the t is set to 0.6, PICA + SVM missed only one case that was GM for Noise 5-rf0 as compared to FCM that missed six

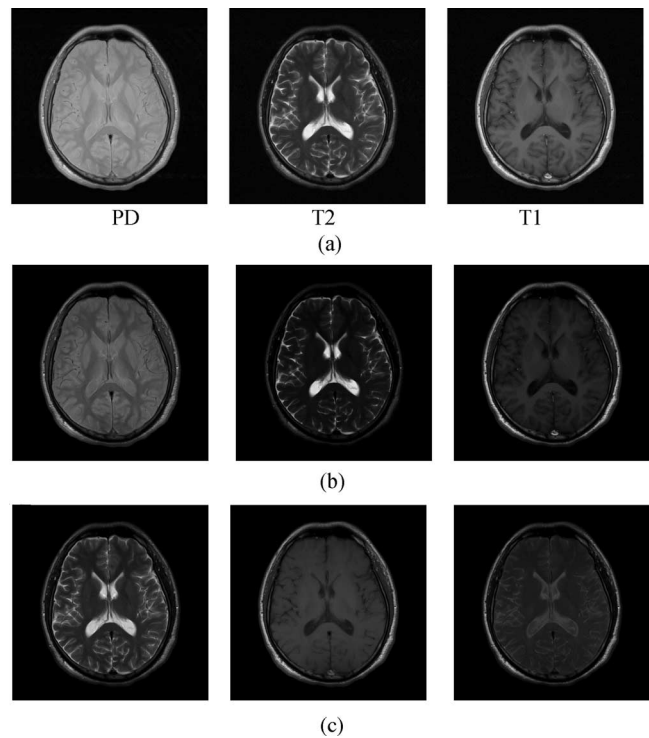


Fig. 5. Real MR brain images and their band images generated by the BEP.

cases (two cases for GM and four cases for WM). In this case, PICA + SVM apparently outperformed FCM.

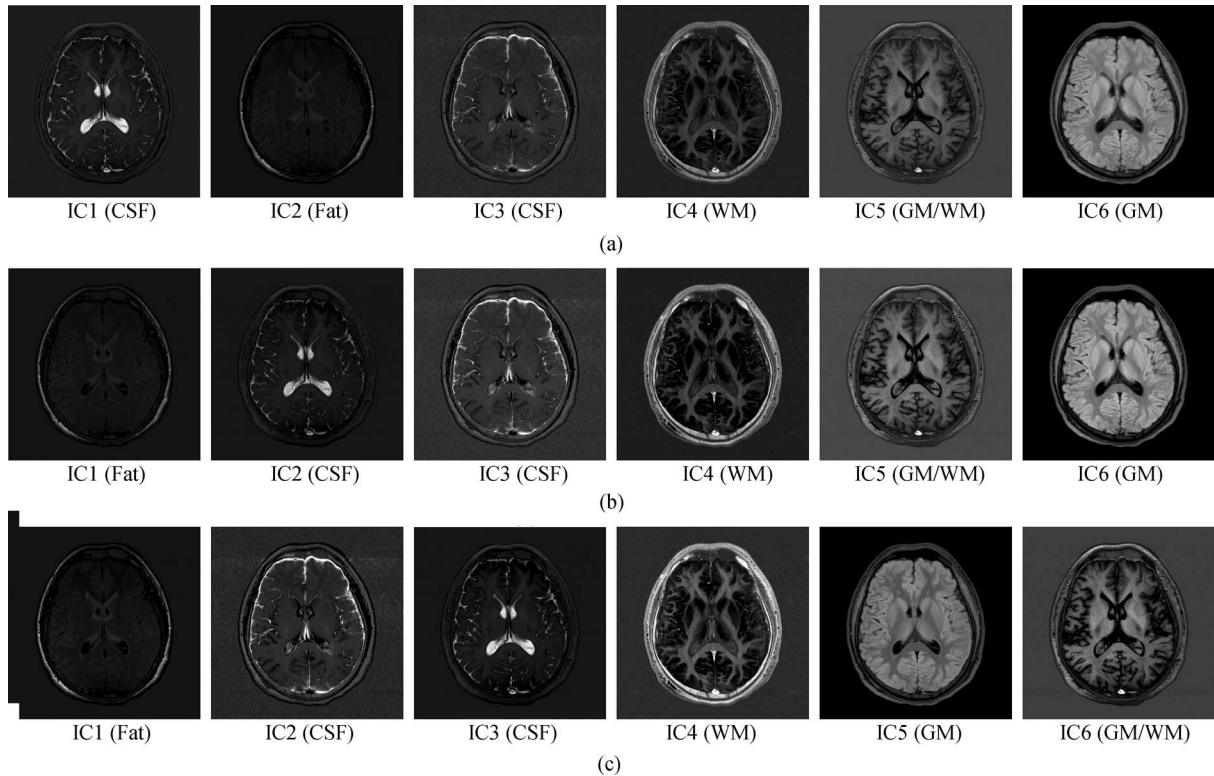


Fig. 6. Six FastICA generated ICs with the BEP expanded images using three different sets of random initial projection vectors.

C. Real MR Brain Image Experiments

In this section, we further demonstrate the utility of the PICA-BEP in real MR image experiments. The real MR brain images were acquired from one normal volunteer by a whole body 1.5-T MR system (Sonata, Siemens, Erlangen, Germany). The routine brain MR protocol consisted of axial spin echo T1 weighted images (TR/TE = 400/9 ms), proton density image (TR/TE = 4000/10 ms), and T2 weighted images (TR/TE = 4000/91 ms). Other imaging parameters included for this study were slice thickness = 6 mm, matrix = 256×256 , field of view (FOV) = 24 cm, number of excitations (NEX) = 2. Since many miscellaneous brain tissue substances in MR brain images cannot be specified *a priori* and also may not have clinical values, only GM, WM, and CSF are of great interest in medical diagnosis. For consistency, the experiments were conducted based on separation of these three brain tissues in the same way as was conducted in [2] and in Section V-B. Fig. 5(a) shows the three MR brain images obtained by T1 weighted, T2 weighted, and proton density images. To reduce head movement, sponge pads were placed on both sides of a patient's head in the head coil during examination. Fig. 5(b) shows three band images generated by BEP using step 2(ii) via crosscorrelation, which were combined with the three original images in Fig. 5(a) to make up a six-band image cube for the ICA to produce six ICs.

Fig. 6 shows three scenarios of six ICs produced by the FastICA using three different sets of random initial projection vectors.

Since the performance using the FastICA on the three original MR images in Fig. 5(a) was very poor, their experiments are not included. As we can see from Fig. 6, the six ICs generated from

three scenarios appeared in different orders. Also observed from the results in Fig. 6, the WM and GM were always classified in the last two ICs, while the CSF was always classified early and split in two separate ICs. It is also interesting to note that according to our experiments, real images in Fig. 5(a) present more challenging issues for clinical diagnosis as compared to synthetic images in Fig. 1(a).

According to Fig. 7(a)–(c) produced by three PICA-BEP algorithms, Eigen-PICA-BEP, HOS-PICA-BEP, and ATGP-PICA-BEP, respectively, the one produced by the Eigen-PICA-BEP was not as good as that by other PICA-BEP algorithms because it could not separate the GM. This is because eigenvalues represent second-order statistics, and they are not good indicators of the presence of target substances characterized by high-order statistics.

Comparing Figs. 7–4, two differences can be observed. One is that all the CSF, WM, and GM in Fig. 7(a)–(c) were prioritized in this order. However, this is not true for Fig. 4 for simulated images, where the CSF might not be the first one prioritized, but, at least, the second prioritized substance. A second difference is that the CSF and GM and WM in real images may be classified into more than one IC instead of a single IC as demonstrated in simulated images. This is mainly due to the fact that there are many unknown substances in real images, which cannot be identified and could be accommodated in various ICs. However, such unknown and unidentified substances could be avoided in simulated images. As a consequence, the classification of the CSF, GM, and WM is more difficult for real images than simulated images, and is generally not as good as the results obtained for simulated images, a fact that makes sense.

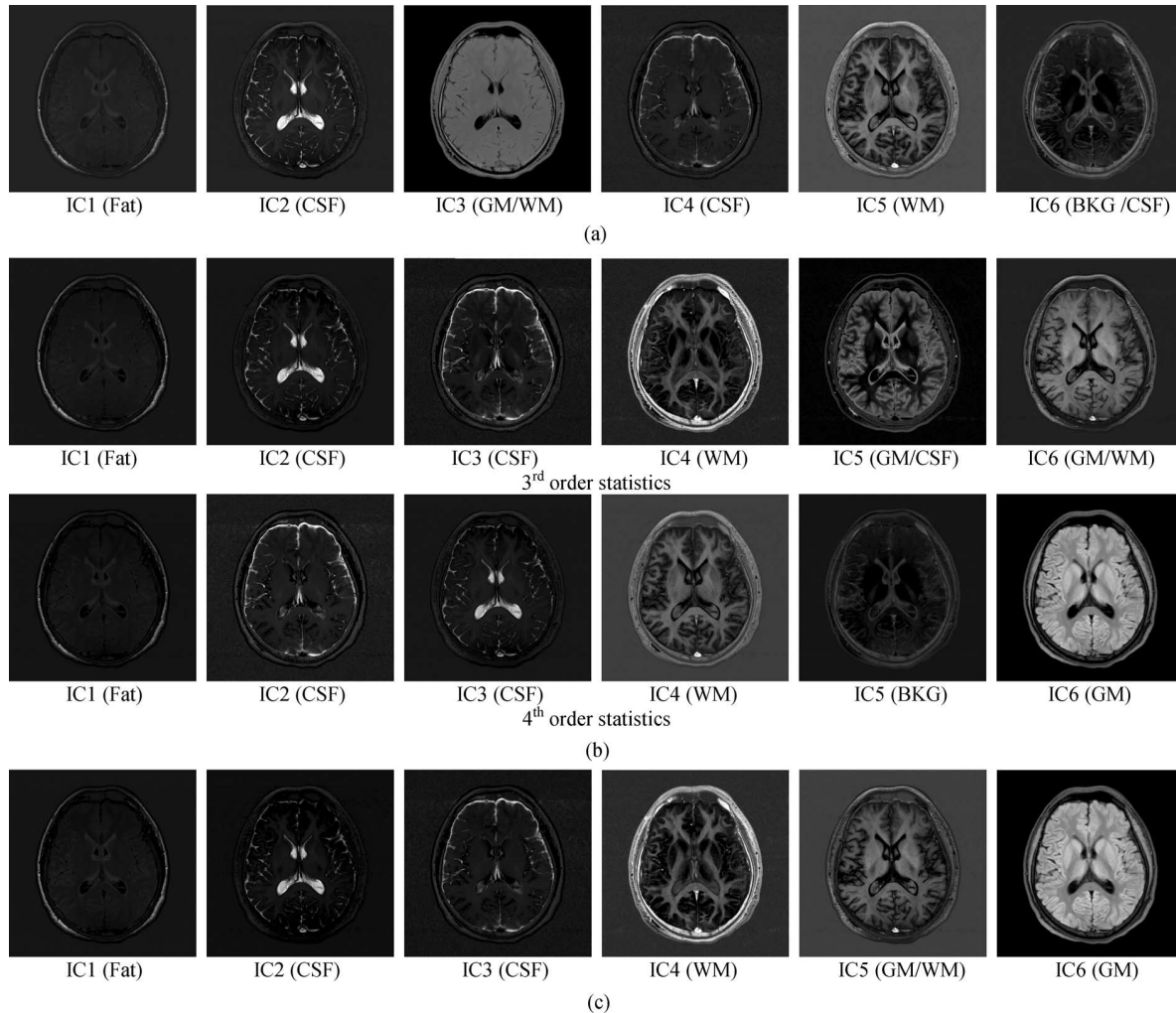


Fig. 7. Results from three PICA-BEP approaches, Eigen-PICA-BEP, HOS-PICA-BEP, ATGP-PICA-BEP.

VI. DISCUSSIONS

As demonstrated by PICA-BEP in experiments, no matter which criterion was used, the priorities of the GM and WM were never higher than three ICs. As a result, if only three MR images were used to accommodate all brain tissue substances, GM and WM would not have high priorities to be accommodated in these three ICs. As a result, they would be very much likely to be scrambled with other substances in the only three available ICs. In this case, the BEP becomes an effective means of mitigating this problem, as demonstrated by results in Figs. 3 and 4 and Figs. 6 and 7, where BEP created three additional new ICs to successfully accommodate the GM and WM. Seven observations from the experiments conducted in Sections V-A–V-C are noteworthy.

1) In all experiments conducted in this paper, only the three band images generated by BEP via crosscorrelation in step 2(ii) were used in conjunction with the three original MR brain images for experiments. According to our extensive experiments, it seems that these three crosscorrelation-generated band images already provide sufficient information to effectively separate the three major brain tissues, GM, WM, and CSF in different ICs.

2) Experiments were also conducted by incorporating only the three band images that were generated by BEP using step 2(i) via autocorrelation with the original images. It turned out that the results using autocorrelation-generated band images were not as good compared to those using crosscorrelation-generated band images. The reason is very obvious that self-correlated information is not as useful as crosscorrelated information obtained by correlating two different band images.

3) Experiments combining three autocorrelated and three crosscorrelated expanded images generated by BEP using both steps 2(i) and 2(ii) were also performed in comparison with the results presented in this section. The results also show no visible improvement, and thus, they are not included here. This is due to limitation of effectiveness of using BEP to generate new images from the three original images. When only three MR images are used, BEP reaches at a point that three additional images are sufficiently enough and there is not much gain that can be benefited by including more nonlinear self-correlated images. However, it has been shown in [3] that if there are four original multispectral images, BEP may need to

generate more additional images to extend and improve its performance. This suggests that the number of additional images for BEP to generate is determined by the number of the original multispectral images. For three MR images, three BEP-generated images may suffice as demonstrated in the experiments in Section V.

- 4) BEP is a powerful technique, which can self-clone images from a set of original multispectral images. However, it should be noted that the BEP cannot be over done. A danger of this practice may result in over-separation in the sense that a substance is forced to be split and separated in more ICs. Therefore, as a guide of using BEP for three-band MRI analysis, it is recommended that using crosscorrelated band images for BEP may be good enough to accommodate our needs.
- 5) It is worth noting that ICA is designed for signal source separation, but not for classification. Therefore, the image experiments conducted in Sections V-A and V-C were evaluated by visual inspection of GM, WM, and CSF separated in different and individual ICs not by classification. However, in order to perform quantitative analysis in Section V-B, the ICs must be thresholded for quantification. This is because the values in all ICs are real valued. In doing so, SVM was chosen to quantify the results due to its ability in classification.
- 6) As noted earlier, the values in ICA-generated ICs are real values to reflect the detected abundance fractions of brain tissue substances by blind separation. Therefore, the abundance fractions of the same brain tissue substances can be spread over more than one IC, as shown in Figs. 3 and 4 and Figs. 6 and 7. This phenomenon is particularly evidential for CSF. As a result, PICA performed poorer than C-means and FCM methods in separation of CSF. Such situation became even worse when BEP was used to expand MR images, in which case, PICA-BEP split CSF in more ICs via BEP. Consequently, PICA-BEP performed worse than PICA without BEP, as demonstrated in Table I(a) and (b). This may explain why Nakai *et al.* did not discuss the CSF in [2] due to its poor performance. However, at the expense of its poor performance in CSF separation, PICA-BEP significantly improved its ability in separation of GM and WM, as shown in Table I(a) and (b), Figs. 3 and 4 and Figs. 6 and 7.
- 7) Since ICA separates brain tissue substances by detecting their abundance fractions, ICA is not a classification, but rather a separation method. In order to make ICA a classification technique, the ICA needs to be implemented in conjunction with a classifier as a postprocessing step to produce a classification map.

VII. CONCLUSION

ICA is a versatile technique and has been found in many applications. However, it cannot be blindly applied without extra care. This paper demonstrates that the commonly used UC-ICA based on under representation of a mixing model cannot be directly applied to MRI analysis, which actually deals with

OC-ICA. This paper presents a new application of OC-ICA in MRI analysis, which has not been explored in the past. In particular, it addresses two key issues arising in UC-ICA, insufficient MR images and inconsistent results caused by the use of random initial projection vectors used in ICA by introducing two new concepts, the BEP to resolve the first issue and PICA to mitigate the second issue. A combination of the BEP and PICA results in a new OC-ICA approach, called PICA-BEP that can be used for MRI analysis in the sense that brain tissue substances of interest can be separated in individual ICs for contrast enhancement. The experimental results show that PICA-ICA improves the traditional UC-ICA and spatial domain-based analysis techniques such as C-means.

REFERENCES

- [1] A. Hyvarinen, J. Karhunen, and E. Oja, *Independent Component Analysis*. Hoboken, NJ: Wiley, 2001.
- [2] T. Nakai, S. Muraki, E. Bagarinao, Y. Miki, Y. Takehara, K. Matsuo, C. Kato, H. Sakahara, and Isoda, "Application of independent component analysis to magnetic resonance imaging for enhancing the contrast of gray and white matter," *NeuroImage*, vol. 21, pp. 251–260, 2004.
- [3] H. Ren and C.-I Chang, "A generalized orthogonal subspace projection approach to unsupervised multispectral image classification," *IEEE Trans. Geosci. Remote Sens.*, vol. 38, no. 6, pp. 2515–2528, Nov. 2000.
- [4] J. Wang and C.-I Chang, "Independent component analysis-based dimensionality reduction with applications in hyperspectral image analysis," *IEEE Trans. Geosci. Remote Sens.*, vol. 44, no. 6, pp. 1586–1600, Jun. 2006.
- [5] A. J. Bell and T. J. Sejnowski, "An information-maximization approach to blind separation and blind deconvolution," *Neural Comput.*, vol. 7, pp. 1129–1159, 1995.
- [6] A. Hyvarinen and E. Oja, "A fast fixed-point for independent component analysis," *Neural Comput.*, vol. 9, no. 7, pp. 1483–1492, 1997.
- [7] <http://www.cis.hut.fi/projects/ica/fastica>
- [8] L. L. Scharf, *Statistical Signal Processing*. Reading, MA: Addison-Wesley, 1991.
- [9] J. C. Harsanyi and C.-I Chang, "Hyperspectral image classification and dimensionality reduction: An orthogonal subspace projection approach," *IEEE Trans. Geosci. Remote Sens.*, vol. 32, no. 4, pp. 779–785, Jul. 1994.
- [10] <http://www.bic.mni.mcgill.ca/brainweb/faq.html#protocols>
- [11] S. Theodoridis and K. Koutroumbas, *Pattern Recognition*. New York: Academic, 1999, pp. 366–368.
- [12] J. S. Jang, C. T. Sun, and E. Mizutani, *Neuro-Fuzzy and Soft Computing: A Computational Approach to Learning and Machine Intelligence*. Upper Saddle River, NJ: Prentice-Hall, 1997.
- [13] S. Haykin, *Neural Networks: A Comprehensive Foundation*, 2nd ed. Upper Saddle River, NJ: Prentice-Hall, 1999, Ch. 6.
- [14] <http://ida.first.fraunhofer.de/~anton/software.html>
- [15] R. Valdes-Cristerna, V. M. Banuelos, and O. Yanez-Suarez, "Coupling of radial basis networks and active contour model for multispectral brain MR images," *IEEE Trans. Biomed. Eng.*, vol. 51, no. 3, pp. 459–470, Mar. 2004.



Yen-Chieh Ouyang (S'86–M'92) received the B.S.E.E. degree in electrical engineering from Feng Chia University, Taiwan, Taichung, R.O.C., in 1981, and the M.S. and Ph.D. degrees in electrical engineering from the University of Memphis, Memphis, TN, in 1987 and 1992, respectively.

Since 1992, he has been with the Department of Electrical Engineering, National Chung Hsing University, Taichung, where he is currently is an Associate Professor and the Director of the Multimedia Communication Laboratory. His current research interests include hyperspectral image processing, medical imaging, communication networks, network security in mobile networks, multimedia system design, and performance evaluation.



Hsian-Min Chen received the B.S. and M.S. degrees in industrial engineering and management information from Huafan University, Taipei, Taiwan, R.O.C., in 1999 and 2001, respectively. He is currently working toward the Ph.D. degree at the Department of Electrical Engineering, National Chung Hsing University, Taichung, Taiwan.

His current research interests include digital image processing and biomedical image processing.



Jyh-Wen Chai received the M.D. and Ph.D. degrees in biomedical engineering from the National Yang-Ming Medical School, Taipei, Taiwan, R.O.C., in 1984 and 2002, respectively.

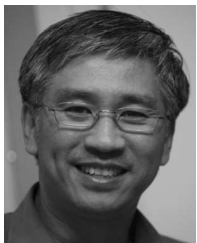
He is currently the Section Chief in the Department of Radiology, Veterans General Hospital, Taichung, Taiwan, and an Assistant Professor in the School of Medicine, China Medical University, Taichung, Taiwan. His current research interests include biomedical image processing, computed tomography (CT), magnetic resonance imaging (MRI), and function MRI.



Clayton Chi-Chang Chen received the M.D. degree in medicine from China Medical College, Taichung, Taiwan, R.O.C., in 1981.

He is currently the Chairman in the Department of Radiology, Veterans General Hospital, Taichung, and an Associate Professor in the Department of Radiological Technology, Central Taiwan University of Science and Technology, Department of Physical Therapy, Hungkung University of Technology, Taichung, and the Department of Physical Therapy, National Yang-Ming University, Taipei, Taiwan. His current

research interests include biomedical image analysis, neuroradiology, computed tomography (CT), magnetic resonance imaging (MRI), and function MRI.



Sek-Kwong Poon received the B.S. degree in biology from the University of Hong Kong, Hong Kong, in 1980, and the M.B.B.S. degree in medicine and surgery from China Medical University, Taichung, Taiwan, R.O.C., in 1987.

He was qualified in Board of Internal Medicine and Board of Gastroenterology and Hepatology, Taiwan, in 1991 and 1994, respectively. He is currently a Clinical Staff in the Department of Gastroenterology and the Head of Clinical Informatics Research and Development Center, Taichung Veterans

General Hospital, Taichung. His current research interests include hepatology, gastroenterology, image processing, clinical informatics, and patient safety.



Ching-Wen Yang received the B.S. degree in information engineering sciences from Feng-Chia University, Taichung, Taiwan, R.O.C., in 1987, and the M.S. degree in information engineering in 1989 and Ph.D. degree in electrical engineering in 1996 both from the National Cheng Kung University, Tainan, Taiwan.

He is currently the Head of the Computer and Communication Center, Taichung Veterans General Hospital, Taichung. His current research interests include image processing, biomedical image processing, and computer network.



San-Kan Lee received the M.D. degree in medicine from the National Defense Medical Center, Taipei, Taiwan, R.O.C., in 1973.

From 1976 to 1989, he was with the Tri-Service General Hospital, Taipei, as a Resident, a Visiting Staff, and the Director of Division of Diagnostic Ultrasound. During 1982, he was a Clinical Fellowship Trainee at the Division of Diagnostic Ultrasound, Thomas Jefferson University Hospital, Philadelphia, PA. During 1990–2003, he was the Chairman of the Department of Radiology, Taichung Veterans General Hospital, Taichung, Taiwan. During 2004, he was the President at Suao Veterans Hospital, Yilan County, Taiwan. Since 2006, he has been with Chia Yi Veterans Hospital, Chia Yi, Taiwan, where he is currently the President. He is also a Professor of Radiology at the National Defense Medical Center, Taipei, and Chung Shan Medical University, Taichung. He is the author or coauthor of more than 200 peer-reviewed papers, and presented more than 50 abstracts in the international conferences. He holds one U.S. and one Taiwan patent. His current research interests include computed-aided diagnosis (CAD) in X-ray mammograms, ultrasound screening of breast cancer, picture archiving and communicating system, and computed tomography.



Chein-I Chang (S'81–M'87–SM'92) received the B.S. degree from Soochow University, Taipei, Taiwan, R.O.C., in 1973, the M.S. degree from the Institute of Mathematics, National Tsing Hua University, Hsinchu, Taiwan, in 1975, the M.A. degree from the State University of New York, Stony Brook, in 1977, all in mathematics, the second M.S. and M.S.E.E. degrees in theoretical computer science and electrical engineering from the University of Illinois, Urbana-Champaign, in 1980 and 1982, respectively, and the Ph.D. degree in electrical engineering from

the University of Maryland, College Park, in 1987.

Since 1987, he has been with the University of Maryland, Baltimore, where he is currently a Professor in the Department of Computer Science and Electrical Engineering. During 1994–1995, he was a Visiting Research Specialist in the Institute of Information Engineering, National Cheng Kung University, Tainan, Taiwan. During 2002–2003, he was a National Research Council (NRC) Senior Research Associateship Awardee. During 2005–2006, he was a Distinguished Lecturer Chair at the National Chung Hsing University, and is currently the Chair Professor at the Environmental Restoration and Disaster Reduction Research Center and Department of Electrical Engineering, National Chung Hsing University, Taichung, Taiwan. He holds three patents and several pending. He was earlier a Guest Editor and a Co-Guest Editor of the *Journal of High Speed Networks*, and currently, on the editorial board. His was also a Co-Guest Editor of the *International Journal of High Performance Computing Applications*. He is the author or coauthor of a book *Hyperspectral Imaging: Techniques for Spectral Detection and Classification* (Kluwer, 2003), and edited two books, *Recent Advances in Hyperspectral Signal and Image Processing*, (Research Signpost, 2006) and *Hyperspectral Data Exploitation: Theory and Applications* (Wiley, 2007). His current research interests include multispectral/hyperspectral image processing, automatic target recognition, medical imaging, information theory and coding, signal detection and estimation, and neural networks.

Prof. Chang was an Associate Editor for IEEE TRANSACTION ON GEOSCIENCE AND REMOTE SENSING (2001–2007) and a Fellow of the International Society for Optical Engineers (SPIE) and a member of Phi Kappa Phi and Eta Kappa Nu.